Single particle tracking of fluorescent nanodiamonds in cells and organisms

Yuen Yung Hui, Wesley Wei-Wen Hsiao, Yung Yuen, Wei-Wen Hsiao, Simon Haziza, Michel Simonneau, François Treussart, Huan-Cheng Chang

▶ **To cite this version:**

Yuen Yung Hui, Wesley Wei-Wen Hsiao, Yung Yuen, Wei-Wen Hsiao, Simon Haziza, et al.. Single particle tracking of fluorescent nanodiamonds in cells and organisms. Current Opinion in Solid State and Materials Science, 2017, 21 (1), pp.35-42. ⟨10.1016/j.cossms.2016.04.002⟩. ⟨hal-03133659⟩

HAL Id: hal-03133659

https://hal.science/hal-03133659v1

Submitted on 6 Feb 2021

HAL is a multi-disciplinary open access archive for the deposit and dissemination of scientific research documents, whether they are published or not. The documents may come from teaching and research institutions in France or abroad, or from public or private research centers.

L'archive ouverte pluridisciplinaire **HAL**, est destinée au dépôt et à la diffusion de documents scientifiques de niveau recherche, publiés ou non, émanant des établissements d'enseignement et de recherche français ou étrangers, des laboratoires publics ou privés.

HAL Authorization

Single particle tracking of fluorescent nanodiamonds in cells and organisms

Yuen Yung Hui[a], Wesley Wei-Wen Hsiao[a], Simon Haziza[b,c], Michel Simonneau[c], François Treussart[b,*], Huan-Cheng Chang[a,d,*]

[a]*Institute of Atomic and Molecular Sciences, Academia Sinica, Taipei 106, Taiwan*

[b]*Laboratoire Aimé Cotton, CNRS, Univ. Paris-Sud, ENS Cachan, Université Paris-Saclay, 91405 Orsay, France*

[c]*Centre de Psychiatrie et Neurosciences, INSERM U894, Université Paris Descartes, 75014 Paris, France*

[d]*Department of Chemical Engineering, National Taiwan University of Science and Technology, Taipei 106, Taiwan*

*Correpsonding authors. E-mail addresses: hchang@gate.sinica.edu.tw; francois.treussart@ens-cachan.fr

Highlights

- Single particle tracking enables nanoscale investigation of cellular processes.
- Fluorescent nanodiamond contains nitrogen-vacancy centers as photostable emitters.
- Background-free imaging and tracking are achievable with nitrogen-vacancy centers.
- Fluorescent nanodiamonds are suitable for long-term tracking in whole organisms.

Abstract

Ever since the discovery of fullerenes in 1985, nanocarbon particles have found a wide range of applications in various areas of science and engineering. Compared with metal, oxide, and semiconductor nanoparticles, the carbon-based nanomaterials have distinct advantages in biomedical applications due to their inherent biocompatibility. Fluorescent nanodiamond (FND) joined the nanocarbon family in 2005. It was initially developed as a contrast agent for bioimaging because it can emit bright red photoluminescence from negatively charged nitrogen-vacancy centers built in the diamond matrix. A notable application of this technology is to study the cytoplasmic dynamics of living cells by tracking single bioconjugated FNDs in intracellular medium. This article provides a critical review on recent advances and developments of the single particle tracking (SPT) research. It summarizes SPT and related studies of FNDs in cells (such as cancer cell lines) and organisms (including zebrafish embryos, fruit fly embryos, whole nematodes, and mice) using assorted imaging techniques.

Keywords

Carbon-based nanomaterial; Fluorescence lifetime imaging microscopy; Magnetic modulation; Nitrogen-vacancy center; Optically detected magnetic resonance

1. Introduction

Biological systems are dynamic in nature. Over the past few decades, several microscopic techniques have been developed to study biological dynamics at the molecular level, including single particle tracking (SPT), fluorescence correlation spectroscopy (FCS), fluorescence recovery after photobleaching (FRAP), and Förster resonance energy transfer (FRET), etc. [1]. However, only the SPT approach allows direct monitoring of the movement of molecules or

vesicles in biological matrices [2, 3]. The technique measures trajectories of these entities and quantifies their Brownian diffusions, confined motions, and directed transports. It enables high-precision longitudinal tracking of the fate of the transported molecules or vesicles not only in single cells but also in whole organisms. Since its first introduction in the late 1980's, SPT in combination with super-resolution imaging at present has become a key technology for quantitative analysis of intra- and inter-cellular processes at the nanometer scale [4].

A nanomaterial useful for SPT applications is fluorescent nanodiamond (FND) [5], which has received increasing attention in recent years for its excellent biocompatibility and superlative optical properties [6, 7]. The negatively charged nitrogen-vacancy (NV^-) defect centers embedded deep in the diamond matrix are responsible for the fluorescence emission. The center is unique in that it can emit bright far-red fluorescence at ~700 nm when excited by green-yellow light and nearly 70% of the emission lies in the near-infrared (NIR) window of biological tissue [8]. Additionally, the fluorescence is perfectly photostable without bleaching and blinking [9], making FND an ideal nanoprobe for long-term imaging and tracking applications. It is especially suitable for use as a contrast agent for following intra- and inter-cellular communications by SPT.

In SPT by fluorescence imaging, laser illumination of biological samples always produces high autofluorescence background that can interfere with the FND detection and lower the observed signal-to-noise ratios. One parameter that can be manipulated to enhance the image contrast of FNDs in physiological environment is the fluorescence lifetime of NV^-. In nanoscale diamond, NV^- has a relatively long lifetime, which is up to 20 ns for FNDs in water and biological buffers (**Fig. 1**) [9 – 12]. This lifetime is substantially longer than that (typically 1 – 4 ns) of cell and tissue autofluorescence [13]. Therefore, time-gating fluorescence imaging or fluorescence lifetime imaging microscopy (FLIM) [14] can be fruitfully applied to eliminate the autofluorescence background when probing single FNDs in cells and organisms.

Another approach that has been undertaken to achieve background-free imaging is to utilize the magnetic properties of the NV^- centers based on a technique known as optically detected magnetic resonance (ODMR) [15]. The method takes advantage of the fact that the spin polarization of NV^- at the ground electronic state (^3A) can be established by optical pumping to the excited state, ^3E. A decrease of the fluorescence intensity results when the center is exposed to the microwave radiation in resonance with the $m_s = 0 \rightarrow m_s = \pm 1$ transitions of the ^3A state at 2.87 GHz. In this method, confocal or wide-field fluorescence images are first acquired with or without the 2.87 GHz microwave irradiation (**Fig. 2**), and subsequent subtraction of the data between these two images at every pixel yields selective images of the FNDs even in high background [16, 17].

The third strategy also exploits the fluorescence intensity variation of NV^- due to the change in relative populations at different m_s sublevels. However, instead of using microwave radiation, the fluorescence intensity variation is induced by applying a modulated magnetic field which creates a mixture of $m_s = 0$ and $m_s = \pm 1$ sublevels [18, 19]. Only the FND fluorescence displays such a modulation but not the surrounding biological environment. Using lock-in detection, the signal of FNDs in a mouse tissue has been retrieved with a 100-fold increase in signal-to-noise ratio compared to the direct detection [19]. The efficient penetration of magnetic fields through tissues makes this approach particularly appealing for whole animal imaging.

This article provides a focused review on SPT of FNDs in biological matrices by confocal and wide-field fluorescence imaging in combination with advanced optical techniques including FLIM and ODMR. It is demonstrated and illustrated how these methods can be applied to probe the dynamics of the carbon-based nanoparticles in cells and organisms with high precision and resolution. Promises and potentials of the NV-enabled nanotechnology for tracking of single FND-labeled cells *in vivo* are also discussed.

2. SPT in cells

The first application of FNDs for SPT in cells appeared in 2007. Fu et al. [9] introduced the particles into cells by endocytosis and managed to track the motion of a single FND (35 nm in diameter) in a living HeLa cell in two dimensions. The same team subsequently improved the SPT technology by mounting a microscope objective lens vertically on a *z*-motion piezoelectric translational stage to monitor the movement of the targeted FND within the depth of field in three dimensions (3D) [20]. **Fig. 3** displays a typical result of the SPT for a bare FND in a HeLa cell. An analysis of the 3D trajectories for more than 200 s revealed a diffusion coefficient comparable to that of the quantum dots confined within endosomal or lysosomal compartments. The high brightness of the particles allowed two-photon excited fluorescence imaging of single 100-nm FNDs using an 875 nm femtosecond laser for illumination inside the cells [20].

In addition to SPT, FNDs with a size in the range of 50 nm can also be probed individually with high image contrast using FCS, which analyzes the correlation of the fluorescence intensity fluctuation of the particles within a tightly focused region [21, 22]. By encapsulating 40 nm FNDs in a lipid layer, Hui et al. [22] showed that the diffusion of the particles in the cytoplasm of a HeLa cell can be enhanced by more than one order of magnitude, compared with that of bare FNDs. This technique together with SPT by one-photon or two-photon excitation has enabled researchers to probe both the short-term and long-term dynamics of the individual FNDs after covalent conjugation with bioactive molecules such as folic acids in living cells [23].

Recently, using again SPT, Epperla et al. [24] demonstrated that FNDs can mediate protein transport through membrane tunneling nanotubes (TNTs) formed between human cells, such as human embryonic kidney cells (HEK293T). TNTs are recently discovered intercellular

communication pathways through which transport of proteins and other cytoplasmic components occurs. They are typically 30 μm in length and 1 μm in diameter, which is large enough to allow 100 nm particles to travel through. In this study, the researchers first modified the FND's surface by covalent conjugation with positively charged poly-arginine (PA) as the buffer layer. Enhanced green fluorescent protein (EGFP) molecules were then non-covalently attached to the PA-grafted FND to form an EGFP-PA-FND complex. The complex was finally coated with bovine serum albumin (BSA) to avoid particle aggregation in cell medium. Prior to the observation, the HEK293T cells were first fed with BSA-coated EGFP-PA-FNDs and then cultured overnight for TNT formation. Given in **Fig. 4** is an example of the active transport of the nanoparticle bioconjugates through a TNT, observed by using a confocal fluorescence microscope. Two-color imaging allowed simultaneous observations of EGFP and FND fluorescence. Analysis of the time-lapse series revealed that the BSA-coated EGFP-PA-FNDs are internalized by endocytosis and ends up inside a cargo which traffics from the cytoplasm of one cell towards the other through the connecting membrane nanotubes. Moreover, the cargoes that contain EGFP-loaded FNDs have a molecular-motor-mediated motion inside the nanotubes with stop and go phases. Furthermore, some cargoes can move along the same TNT in both directions. The observations corroborate the suggestion that the photostable FND is useful not only for delivering biomolecules from one cell to the other but also for long-term tracking of the delivery.

Another SPT application of FNDs in living cells was recently carried out by Liu et al. [25]. In this work, 40 nm FNDs were conjugated with transforming growth factor (TGF) that directs the complexes towards membrane TGF-β receptors. FCS measurements estimated an average hydrodynamic diameter of 46 nm for BSA-coated TGF-FNDs. By monitoring the 3D motions of these receptors in human lung cancer cells (HCC827) with SPT, the researchers found that the TGF-β displays a highly heterogeneous behavior in the cells with three different states:

immobile, intermediate, and fast diffusion (**Fig. 5**). Upon treatment with small molecule inhibitors (SMI) of kinases, the immobile population significantly decreased while the intermediate and fast populations increased. Additionally, the rates of the transition between these three states significantly changed, leading to the formation of preferred intermediate and fast diffusion states. The researchers concluded that the TGF-β immobilized on FND is essential for active signaling, a result indirectly proving that the tagging of TGF-β with 40 nm FND does not significantly influence the outcome of the transmembrane signaling dynamics in living cells. This work introduces a novel application of FND as specific endogenous protein tags to study intracellular processes.

Aside from tracking the position of a single FND in 3D, the orientation of the particle in a living cell can be monitored by recording its ODMR spectra as a function of time, provided that it contains only a single NV^- center (i.e. a single electron spin) in the lattice. The study is possible because in the presence of an external magnetic field, the ODMR peaks splits into two Zeeman components ($m_s = +1$ and $m_s = -1$) and the magnitude of the splitting depends on the orientation of the individual NV^- with respect to the field. McGuinness et al. [26] have performed a proof-of-principle experiment by applying a uniform magnetic field to 50 nm FNDs internalized by HeLa cells (**Fig. 6**). From a close analysis of the peak positions of the ODMR spectra, information on the rotational motions of the FNDs in the cells could be deduced. Thanks to the perfect photostability of FNDs, the researchers were able to monitor the reorientational dynamics continuously over 16 h.

3. SPT in organisms

To extend the SPT studies from cells to organisms, Chang et al. [27] employed 100 nm FNDs as nanoprobes to explore the cytoplasmic dynamics in zebrafish yolk cells. First, the researchers non-covalently conjugated FNDs with BSA to prevent clustering in phosphate-

buffered saline (PBS). Next, the BSA-coated FNDs were microinjected into the yolk of a zebrafish embryo at the one-cell stage. They found that the FNDs underwent unidirectional and stop-and-go traffic in the yolk cell with a velocity of 0.19 – 0.40 μm/s along the axial streaming. More importantly, these particles could be incorporated into the dividing cells and dispersed in the fish's body when the embryos developed into larvae and subsequently into adult fish. No apparent abnormalities were detected for the FND-injected fishes throughout their embryogenesis. It is concluded that the FNDs may find practical use as photostable non-toxic markers in small animal models.

The SPT of FND has similarly been applied to investigate the embryogenesis of the fruit fly, *Drosophila melanogaster*, a model organism for genetic studies. Again, taking advantage of the excellent photostablility of FND, Simpson et al. [28] introduced BSA-coated FNDs into the embryo and investigated the FND diffusion in both furrow periplasm and sub-nuclear periplasms by SPT (**Fig. 7**). As the NV^- fluorescence can be easily distinguished from the embryo autofluorescence, the researchers were able to observe both the free diffusion and driven motion of the particles in the blastoderm cells at the posterior end of the *Drosophila* embryos during cellularization. From the trajectory analysis, they determined a mean diffusion coefficient of 6×10^{-3} $\mu m^2/s$ and a mean driven velocity of 0.13 μm/s in the furrow periplasm. In the sub-nuclear periplasm, the corresponding diffusion coefficient and driven velocity are 63×10^{-3} $\mu m^2/s$ and 0.27 μm/s, respectively. It indicates that although the transport mechanisms of FNDs are analogous in furrow and sub-nuclear periplasms, their diffusion rates differ by a factor of 10. The difference could be attributed to the fact that the cytoskeletal networks are denser in the furrow periplasm, where the diffusion of FNDs is more significantly inhibited.

The first attempt of conducting SPT of FNDs in whole organisms was made by Igarashi et al. [16], who developed a selective imaging method based on ODMR to improve the image

contrast *in vivo*. In this method, wide-field fluorescence images were first acquired with or without 2.87 GHz microwave irradiation. Then the subtraction between these two images at every pixel was carried out to yield selective images of the FNDs. They took this approach to conduct long-term tracking of ~200 nm FNDs in both nematodes (*C. elegans*) and mice, achieving good image contrast by deleting background autofluorescence signals. To attain better time resolution and faster sampling of photons, the same research team used a spectrometer equipped with an avalanche photodiode for detection, which enabled them to collect fluorescence emission at a sampling rate of up to 20 kHz [29]. They measured the ODMR spectra of FNDs introduced into the intestine of *C. elegans* as an example. Their results showed that the technique can completely eliminate extraneous fluorescence for real-time observations of FNDs. This selective imaging method, although technically challenging, is expected to be applicable to a wide range of living systems.

Time gating serves an alternative approach to achieve background-free detection of FNDs for SPT in whole organisms. Kuo et al. [12] applied this technique to investigate the intercellular transport of yolk lipoproteins in *C. elegans*. In this work, 100 nm FNDs were first non-covalently coated with green fluorescent protein (GFP)-tagged yolk lipoprotein complexes (YLCs) by physical adsorption to form GFP::YLC-conjugated FNDs (GFP::YLC-FNDs). The particles were then microinjected into the anterior intestinal cells near the pharynx. Time-lapse imaging with FLIM by gating the FND fluorescence signals at the time longer than 10 ns allowed background-free detection. More than 25 worms were examined individually to identify the location of GFP::YLC-FNDs in the specific cells or organs over 55 min after injection (**Fig. 8**). Results showed that the GFP::YLC-FND particles appeared in the posterior intestine immediately following administration. They were then observed in the pseudocoelom and the loop region of the gonad at 5 min and 12 min post-injection, respectively. Twenty minutes later, the NV^- fluorescence became visible in the oocytes. More interestingly and

significantly, embryos bearing FNDs were found at 55 min after injection, indicating that the FND-containing oocytes could be fertilized and developed into embryos normally.

The concept of SPT can be readily adapted to tracking of single cells *in vivo*. Hui et al. [30] have presented a new approach to achieve background-free fluorescence imaging of single FND-labeled cells in a mouse model. Here, an intensified charge-coupled device (ICCD) served as the detector. ICCD is a highly sensitive camera capable of high-speed gating operation. It is useful to suppress short-lifetime fluorescence background and provide time-gated fluorescence images with enhanced contrast. Using an ICCD with nanosecond gating resolution and a Raman shifter, the team demonstrated the first application of the device for wide-field fluorescence imaging of FND-labeled cells in living mice. They employed mouse lung cancer cells as the model cell line and introduced the cells after FND labeling into a mouse via tail vein injection. Fluorescence imaging was then carried out in a main blood vessel of the mouse's ear. Shown in **Fig. 9** are typical bright-field and time-gated fluorescence images of the ear tissue. About 10 min after intravenous injection of the particles, bright objects moving at an average speed of 0.4 μm/s could be clearly identified in the blood vessel. This measured speed is much lower than the blood flow velocity by almost 3 orders of magnitude. Thus, it is most likely associated with the rolling, instead of flowing, of the FND-labeled cells in the blood vessel. This time-gating technique is promising for real-time imaging and tracking of transplanted stem cells for tissue repair and regeneration in small animal models.

4. Conclusion and outlook

Owing to its perfect photostability, unique magneto-optical property, and high biocompatibility, FND has been proven to be a useful nanoprobe for SPT in biological matrices with high spatial and temporal resolution. There is little doubt that it will be adopted by researchers to address outstanding challenges hardly accessible with other means. The recent emerging nanoscale

applications of NV^- centers in bioimaging and biosensing clearly support this notion [15, 31]. However, in the context of cellular imaging, the FND-enabled technology is far from ideal. It suffers from the drawback that the particles are large, typically 30 − 100 nm, which prevents their use as first-line molecular tags. Further reduction of the particle size to the 10 nm range without significantly compromising fluorescence brightness is required [32, 33].

Despite being imperfect, the ca. 100 nm FNDs can still find various applications in biology and medicine [34]. For instance, they can be used as long-term trackers of cancer and stem cells thanks to their excellent chemical and photophysical stability [35 – 37]. They may also serve as protein, gene, and drug delivery vehicles due to the ease of their surface modification and their high loading capacities [38 – 40]. Imaging and tracking of fluorescently labeled events *in vivo* can be more easily realized with these high-brightness FND particles as contrast agents. Detection of such FNDs after subcutaneous injection into a rat with a skin thickness of ~2.0 mm has been achieved [8].

In applying FNDs for *in vivo* imaging, while FLIM and ODMR are viable methods to reduce background fluorescence signals, the more practical and promising approach seems to be the magnetic modulation [19]. The efficient penetration of magnetic fields through tissues and the relatively small amplitude required make this approach particularly suited for whole animal imaging, although the limitation of multiple scattering of optical photons when penetrating deep into the tissues remains an issue. However, with further sensitivity improvements, this wide-field technique is expected to allow background-free SPT at an acquisition speed compatible with the recording of intra- or inter-cellular transport processes *in vivo*.

Acknowledgement

This work is supported by Academia Sinica and the Ministry of Science and Technology, Taiwan, with Grant No. 104-2811-M-001-149, as well as by French National Research Agency (ANR) with Grant No. 2010-INTB-1002 and a public grant overseen by ANR as part of the "Investissements d'Avenir" program (Labex NanoSaclay, reference: ANR-10-LABX-0035).

References

[1] Lippincott-Schwartz J, Snapp E, Kenworthy A. Studying protein dynamics in living cells. Nat Rev Mol Cell Biol 2001;2:444-56.

[2] Saxton MJ, Jacobson K. Single-particle tracking: applications to membrane dynamics. Annu Rev Biophys Biomol Struct 1997;26:373-99.

[3] Levi V, Gratton E. Exploring dynamics in living cells by tracking single particles. Cell Biochem Biophys 2007;48:1-15.

[4] Cognet L, Leduc C, Lounis B. Advances in live-cell single-particle tracking and dynamic super-resolution imaging. Curr Opin Chem Biol 2014;20:78-85.

[5] Yu SJ, Kang MW, Chang HC, Chen KM, Yu YC. Bright fluorescent nanodiamonds: no photobleaching and low cytotoxicity. J Am Chem Soc 2005;127:17604-5.

[6] Vaijayanthimala V; Chang HC. Functionalized fluorescent nanodiamonds for biomedical applications. Nanomedicine 2009;4:47-55.

[7] Mochalin VN, Shenderova O, Ho D, Gogotsi Y. The properties and applications of nanodiamonds. Nat Nanotechnol 2011;7:11-23.

[8] Vaijayanthimala V, Cheng PY, Yeh SH, Liu KK, Hsiao CH, Chao JI, et al. The long-term stability and biocompatibility of fluorescent nanodiamond as an *in vivo* contrast agent. Biomater 2012;33;7794-802.

[9] Fu CC, Lee HY, Chen K, Lim TS, Wu HY, Lin PK, et al. Characterization and application of single fluorescent nanodiamonds as cellular biomarkers. P Natl Acad Sci USA 2007;104:727-32.

[10] Faklaris O, Garrot D, Joshi V, Druon F, Boudou JP, Sauvage T, Georges P, Curmi PA, Treussart F. Detection of single photoluminescent diamond nanoparticles in cells and study of the internalization pathway. Small 2008;4:2236-9.

[11] Kuo Y, Hsu TY, Wu YC, Hsu JH, Chang HC. Fluorescence lifetime imaging microscopy of nanodiamonds *in vivo*. Proc SPIE 2013;8635:863503.

[12] Kuo Y, Hsu TY, Wu YC, Chang HC. Fluorescent nanodiamond as a probe for the intercellular transport of proteins *in vivo*. Biomaterials 2013;34:8352-60.

[13] Billinton N, Knight AW. Seeing the wood through the trees: A review of techniques for distinguishing green fluorescent protein from endogenous autofluorescence. Anal Biochem 2001;291:175-97.

[14] Chang CW, Sud D, Mycek MA. Fluorescence lifetime imaging microscopy. Methods Cell Biol 2007;81:495–524.

[15] Schirhagl R, Chang K, Loretz M, Degen CL. Nitrogen-vacancy centers in diamond: nanoscale sensors for physics and biology. Annu Rev Phys Chem 2014;65:83-105.

[16] Igarashi R, Yoshinari Y, Yokota H, Sugi T, Sugihara F, Ikeda K, et al. Real-time background-free selective imaging of fluorescent nanodiamonds *in vivo*. Nano Lett 2012;12:5726-32.

[17] Hegyi A, Yablonovitch E. Molecular imaging by optically-detected electron spin resonance of nitrogen-vacancies in nanodiamond. Nano Lett 2013;13:1173-8.

[18] Chapman R, Plakhotnik T. Background-free imaging of luminescent nanodiamonds using external magnetic field for contrast enhancement. Opt Lett 2013;38:1847-9.

[19] Sarkar SK, Bumb A, Wu X, Sochacki KA, Kellman P, Brechbiel MW, et al. Wide-field *in vivo* background free imaging by selective magnetic modulation of nanodiamond fluorescence. Biomed Opt Express 2014;5:1190-202.

[20] Chang YR, Lee HY, Chen K, Chang CC, Tsai DS, Fu CC, et al. Mass production and dynamic imaging of fluorescent nanodiamonds. Nat Nanotechnol 2008;3:284-8.

[21] Neugart F, Zappe A, Jelezko F, Tietz C, Boudou JP, Krueger A. et al. Dynamics of diamond nanoparticles in solution and cells. Nano Lett 2007;7:3588-91.

[22] Hui YY, Zhang BL, Chang YC, Chang CC, Chang HC, Hsu JH, et al. Two-photon fluorescence correlation spectroscopy of lipid-encapsulated fluorescent nanodiamonds in living cells. Opt Express 2010;18:5896-905.

[23] Zhang B, Li Y, Fang CY, Chang CC, Chen CS, Chen YY, et al. Receptor-mediated cellular uptake of folate-conjugated fluorescent nanodiamonds: a combined ensemble and single-particle study. Small 2009;5:2716-21.

[24] Epperla CP, Mohan N, Chang CW, Chen CC, Chang HC. Nanodiamond-mediated intercellular transport of proteins through membrane tunneling nanotubes. Small 2015;11:6097-105.

[25] Liu W, Yu F, Yang J, Xiang B, Xiao P, Wang L. 3D single-molecule imaging of transmembrane signaling by targeting nanodiamonds, Adv Funct Mater 2016;26:365-75.

[26] McGuinness LP, Yan Y, Stacey A, Simpson DA, Hall LT, Maclaurin D, Prawer S, et al. Quantum measurement and orientation tracking of fluorescent nanodiamonds inside living cells. Nat Nanotechnol 2011;6:358-63.

[27] Chang CC, Zhang B, Li CY, Hsieh CC, Duclos G, Treussart F, Chang HC. Exploring cytoplasmic dynamics in zebrafish yolk cells by single particle tracking of fluorescent nanodiamonds. Proc SPIE 2012;8272:827205.

[28] Simpson DA, Thompson AJ, Kowarsky M, Zeeshan NF, Barson MSJ, Hall LT, et al. *In vivo* imaging and tracking of individual nanodiamonds in drosophila melanogaster embryos. Biomed Opt Express 2014;5:1250-61.

[29] Yoshinari Y, Mori S, Igarashi R, Sugi T, Yokota H, Ikeda K, et al. Optically detected magnetic resonance of nanodiamonds *in vivo*; Implementation of selective imaging and fast sampling. J Nanosci Nanotechnol 2015;15:1014-21.

[30] Hui YY, Su LJ, Chen OY, Chen YT, Liu TM, Chang HC. Wide-field imaging and flow cytometric analysis of cancer cells in blood by fluorescent nanodiamond labeling and time gating. Sci Rep 2014;4:5574.

[31] Balasubramanian G, Lazariev A, Arumugam SR, Duan D. Nitrogen-vacancy color center in diamond – emerging nanoscale applications in bioimaging and biosensing. Curr Opin Chem Biol 2014;20:69-77.

[32] Tisler J, Balasubramanian G, Naydenov B, Kolesov R, Grotz B, Reuter R, et al. Fluorescence and spin properties of defects in single digit nanodiamonds. ACS Nano 2009;3:1959-65.

[33] Mohan N, Tzeng YK, Yang L, Chen YY, Hui YY, Fang CY, et al. Sub-20-nm fluorescent nanodiamonds as photostable biolabels and fluorescence resonance energy transfer donors. Adv Mater 2010;22:842-7.

[34] Vaijayanthimala V, Lee DK, Kim SV, Yen A, Tsai N, Ho D, et al. Nanodiamond-mediated drug delivery and imaging: challenges and opportunities. Expert Opin Drug Deliv 2015;12:735-49.

[35] Fang CY, Vaijayanthimala V, Cheng CA, Yeh SH, Chang CF, Li CL, et al. The exocytosis of fluorescent nanodiamond and its use as a long-term cell tracker. Small 2011;7:3363-70.

[36] Wu TJ, Tzeng YK, Chang WW, Cheng CA, Kuo Y, Chien CH, et al. Tracking the engraftment and regenerative capabilities of transplanted lung stem cells using fluorescent nanodiamonds. Nat Nanotechnol 2013;8:682-9.

[37] Lin HH, Lee HW, Lin RJ, Huang CW, Liao YC, Chen YT, et al. Tracking and finding slow-proliferating/quiescent cancer stem cells with fluorescent nanodiamonds. Small 2015;11:4394-402.

[38] Alhaddad A, Adam MP, Botsoa J, Dantelle G, Perruchas S, Gacoin T. et al. Nanodiamond as a vector for siRNA delivery to Ewing sarcoma cells. Small 2011;7:3087-95.

[39] Chang BM, Lin HH, Su LJ, Lin WD, Lin RJ, Tzeng YK, et al. Highly fluorescent nanodiamonds protein-functionalized for cell labeling and targeting. Adv Funct Mater 2013;23:5737-45.

[40] Slegerova J, Hajek M, Rehor I, Sedlak F, Stursa J, Hruby M, et al. Designing the nanobiointerface of fluorescent nanodiamonds: highly selective targeting of glioma cancer cells. Nanoscale 2015;7:415-20.

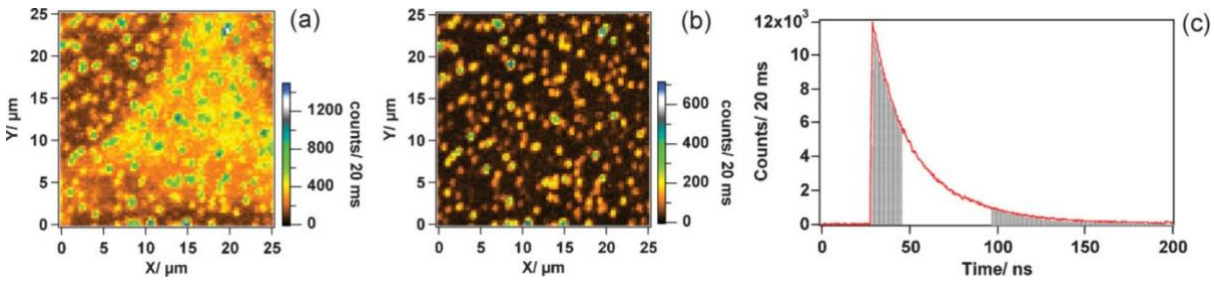

Fig. 1. Time-resolved confocal fluorescence images of a fixed cell containing FNDs. (a) Raster-scan image obtained by detecting all photons, displaying NV^- fluorescence together with cell autofluorescence. (b) Time-gated raster scan constructed from photons detected between 15 and 53 ns after pulsed laser excitation. Scan area: 25 × 25 μm^2. (c) Fluorescence time decay from one of the FNDs shown in (a). (From reference [10])

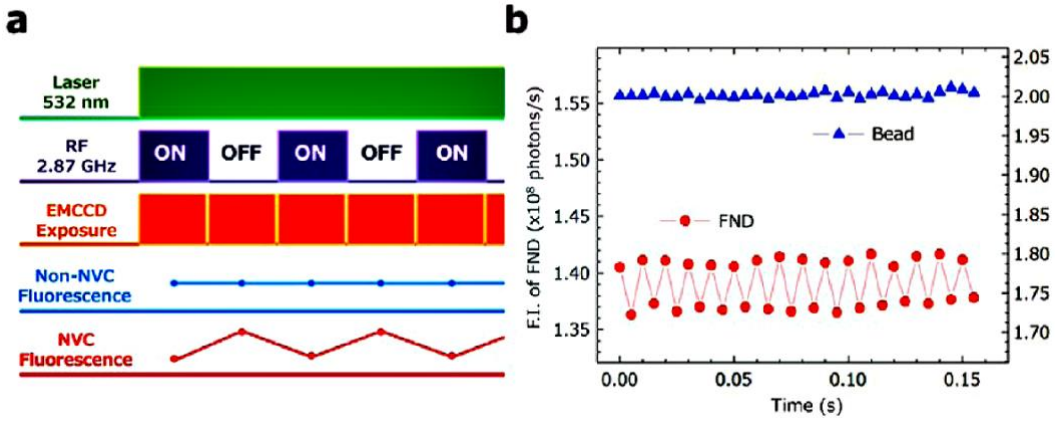

Fig. 2. Background-free detection of FNDs by applying modulated microwave radiation at 2.87 GHz. (a) Time chart of the laser excitation, microwave irradiation, and image acquisition, along with the expected intensity profiles of non-NV and NV fluorescence used for selective imaging of FNDs. (b) Comparison between the time traces of the observed fluorescence intensities of a FND and a fluorescent bead. (From reference [16])

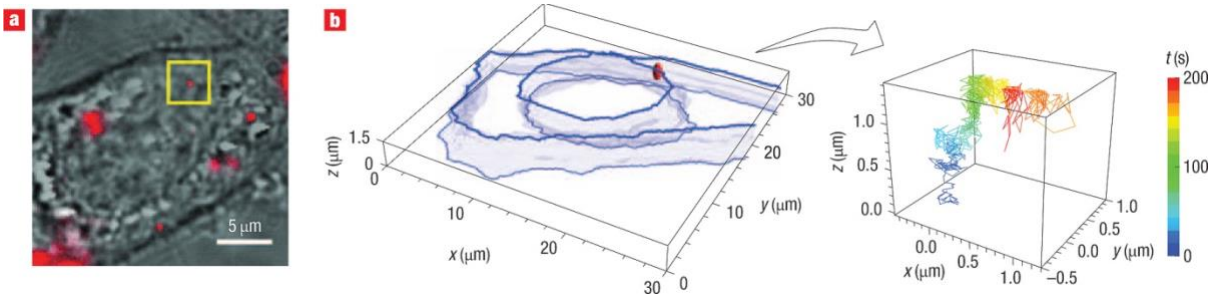

Fig. 3. Three-dimensional tracking of a single FND in a living cell. (a) Merged bright-field and epifluorescence (red) image of the cell after FND uptake. (b) Location (left) and 3D trajectory (right) of the single FND surrounded by a yellow box in (a) over a time span of 200 s. (From reference [20])

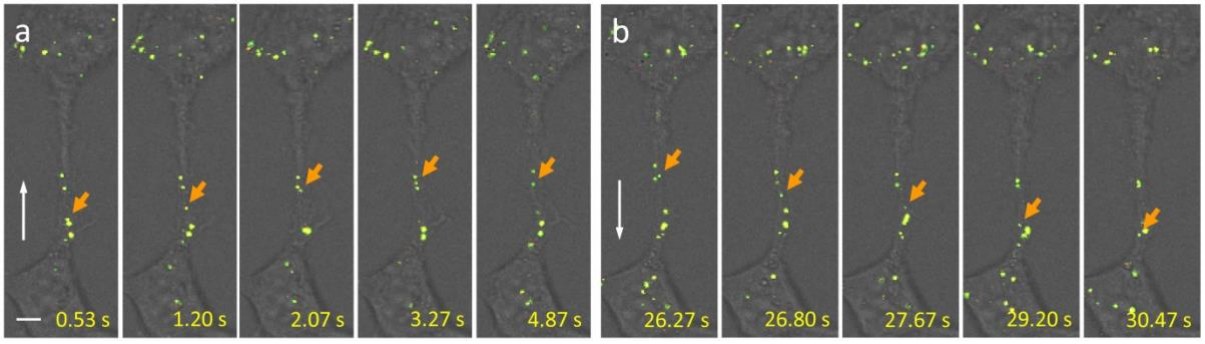

Fig. 4. Tracking of a single EGFP-conjugated FND particle along the connecting membrane nanotube of two living cells. (a) Forward and (b) backward movement of two different particles. White arrows indicate the directions of the particle movement and orange arrows denote the particles of interest in the frames. Scale bar: 5 μm. (From reference [24])

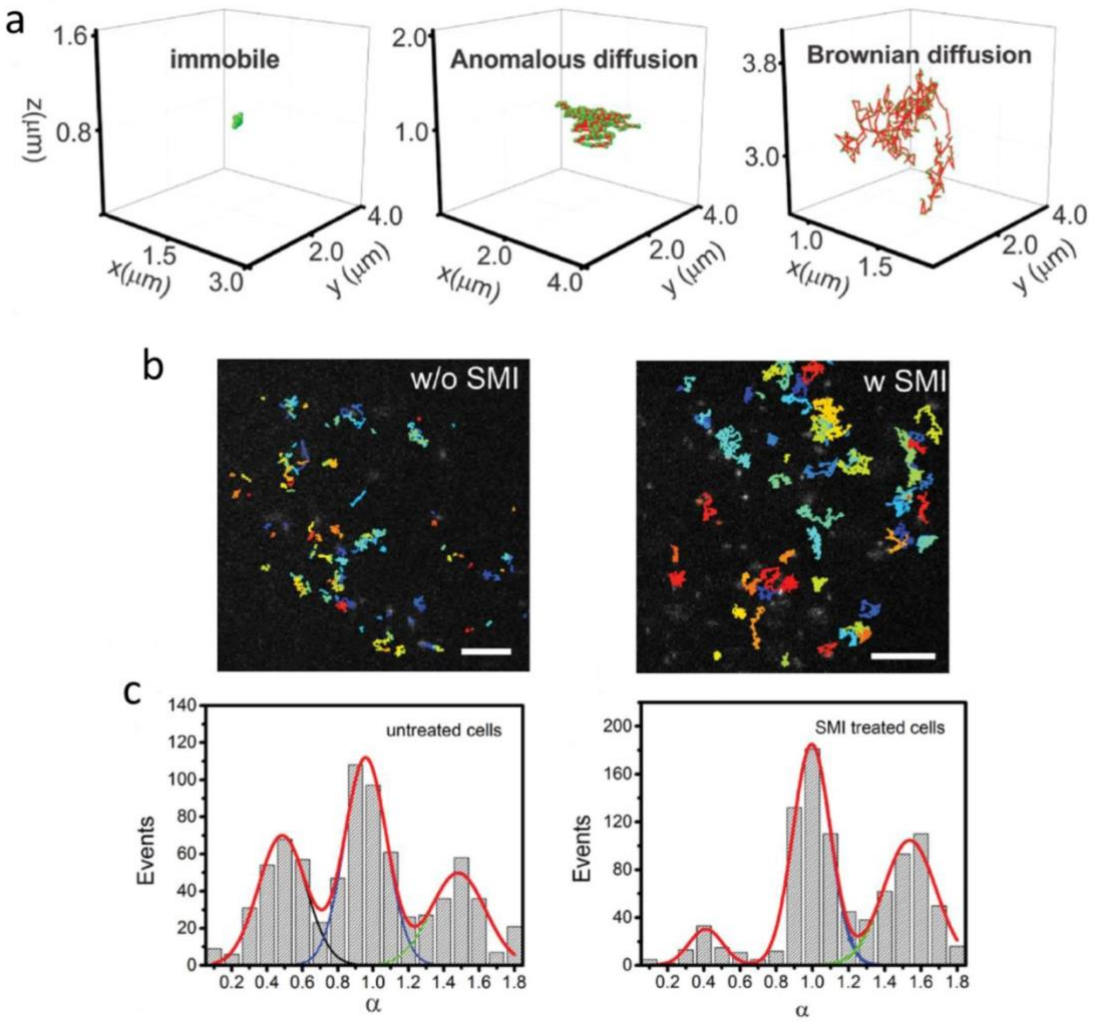

Fig. 5. Single molecule tracking of TGF-β membrane receptors labeled with TGF-conjugated FNDs in living cells. (a) Representative trajectories of the TGF-β: immobile (D = 0.01 μm^2/s), anomalous (D = 0.2 μm^2/s, α = 0.6), and Brownian (D = 3 μm^2/s, α = 0.9), where D is the diffusion coefficient and α is an anomalous diffusion parameter, which is equal to 1 for perfect Brownian diffusion. Data were acquired at 20 Hz for 5 s. (b) TGF-β trajectories overlaid with wide-field fluorescence images without (left) and with (right) the SMI treatment. Color corresponds to the track numbers. Scale bar: 3 μm. (c) Distribution of the values of α in untreated (left) and SMI-treated (right) cells. (From reference [25])

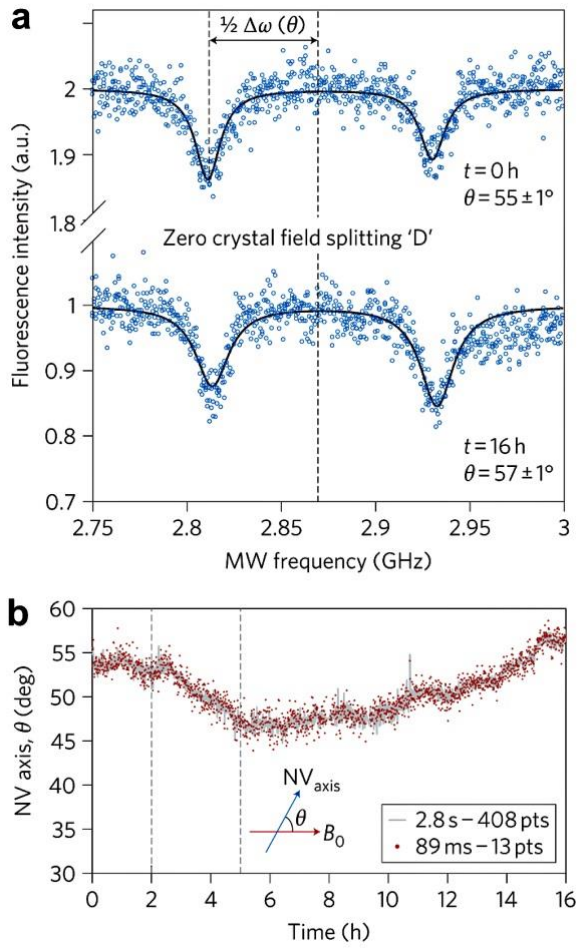

Fig. 6. Orientation tracking of a single FND in a living cell. (a) Changes in orientation of the NV crystallographic axis (also the NV^- spin orientation) relative to an external magnetic field. (b) Measurement of the orientation of the internalized FND as a function of time. (From reference [26])

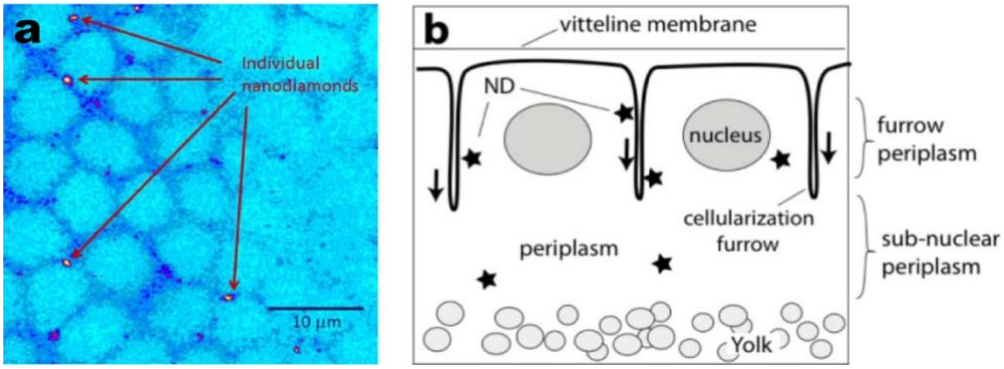

Fig. 7. Tracking of single FNDs in a *Drosophila* embryo. (a) Confocal fluorescence image of individual FNDs in the blastoderm cells during stage 5 of development. (b) Schematic drawing of the structure of an early stage 5 embryo, showing the cellularization furrows introgressing between nuclei, which invade the yolk-free periplasm during the later syncytial divisions indicated as arrows. (From reference [28])

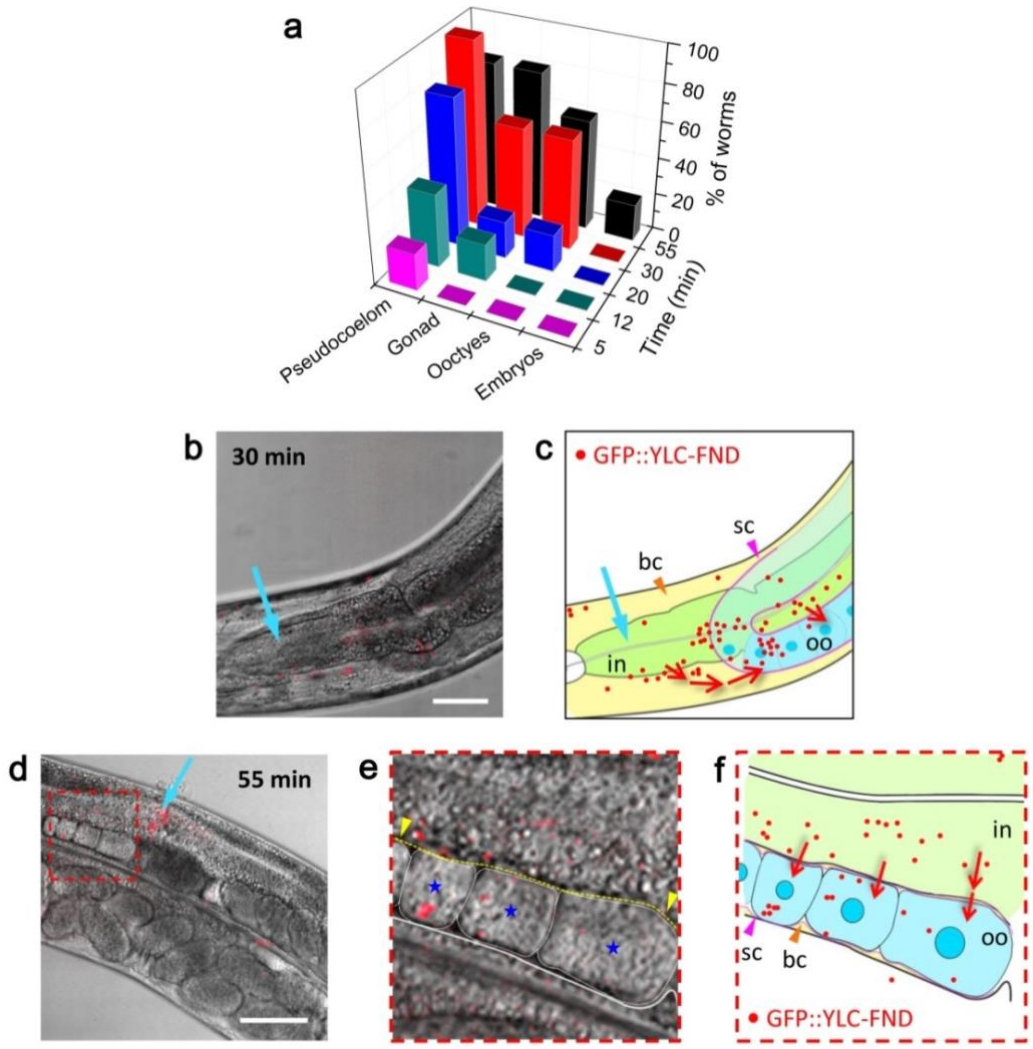

Fig. 8. Tracking the intercellular transport of single FNDs in *C. elegans*. (a) A time-course localization analysis of GFP::YLC-FNDs in specific tissues and organs of the worms over 55 min post-injection. The injection was made at an anterior intestinal cell near the pharynx of each worm. A total of more than 25 worms were examined individually, from which the percentages of the worms showing GFP::YLC-FNDs in the specified tissues and organs were calculated at the indicated time points. (b) A merged bright-field and time-gated fluorescence image of a representative worm at 30 min after injection of GFP::YLC-FNDs into the intestinal cell. (c) A cartoon illustrating the excretion of GFP::YLC-FNDs from the intestine (in) to the body cavity, and after passing through the sheath cells, the excreted GFP::YLC-FNDs enter oocytes. (d) A merged bright-field and time-gated fluorescence image of a representative

worm at 55 min after injection of GFP::YLC-FNDs into the intestinal cell. (e,f) An enlarged image (e) and a cartoon (f) of the area in the red box in (d), showing the presence of GFP::YLC-FNDs in both intestine (with a boundary marked by yellow dotted line) and oocytes (with boundaries marked by thin white lines and nuclei labeled with blue stars). Scale bars are 50 μm. (From reference [12])

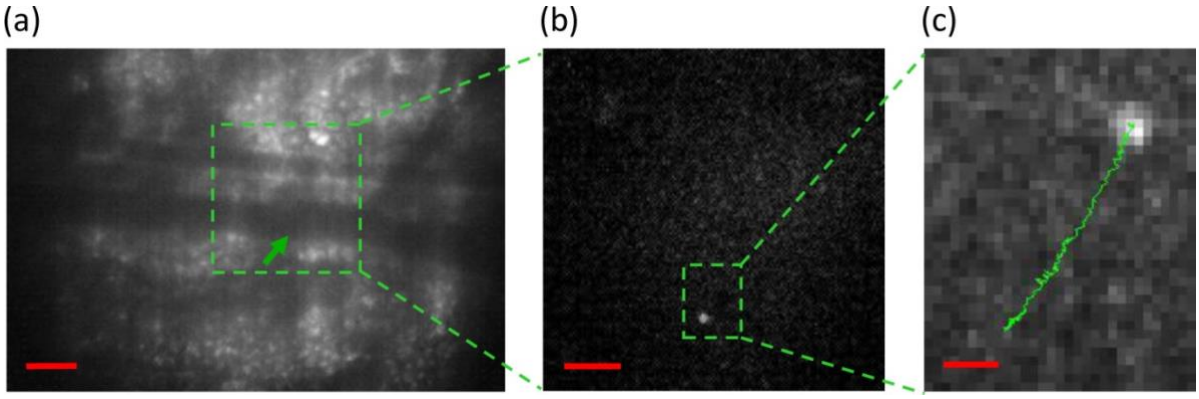

Fig. 9. Tracking of single FND-labeled cells in a mouse ear. (a) Bright-field image of a mouse ear tissue. The green arrow indicates the position of an FND-labeled lung cancer cell in the blood vessel of ~50 μm in diameter. (b) Enlarged view of the fluorescence image of the square green region in (a). The bright spot corresponds to the FND-labeled lung cancer cell. (c) Enlarged view of the fluorescence image of the rectangular green region in (b), showing the trajectory of the FND-labeled lung cancer cell moving in the vessel. The red scale bar corresponds to 100, 50, and 10 μm in (a), (b) and (c), respectively. (From reference [30])

Graphical Abstract